Optimization of GaAs-based 940 nm infrared light emitting diode with dual-junction design*

LIN Hong-liang (林鸿亮)[1,2], **ZENG Xiang-hua** (曾祥华)[1]**, **SHI Shi-man** (石时曼)[2], **TIAN Hai-jun** (田海军)[2], **YANG Mo** (杨默)[2], **CHU Kai-ming** (储开明)[2], **YANG Kai** (杨凯)[2], **and LI Quan-su** (李全素)[2]

1. College of Physics Science and Technology & Institute of Optoelectronic Technology, Yangzhou University, Yangzhou 225002, China

2. Yangzhou Change Light Optoelectronic Co., Ltd., Yangzhou 225009, China

(Received 14 July 2018; Revised 14 August 2018)

Epitaxial growths of the GaAs/AlGaAs-based 940 nm infrared light emitting diodes (LEDs) with dual junctions were carried out by using metalorganic chemical vapor deposition (MOCVD) with different doping concentrations and Al contents in $Al_xGa_{1-x}As$ compound. And their optoelectric properties show that the optimal design for tunneling region corresponds to P^{++} layer with hole concentration up to 1×10^{20} cm^{-3}, N^{++} layer electron concentration up to 5×10^{19} cm^{-3} and constituent $Al_{0.2}Ga_{0.8}As$ in the tunneling junction region. The optimized dual-junction LED has a forward bias of 2.93 V at an injection current of 50 mA, and its output power is 24.5 mW, which is 104% larger than that of the single junction (12 mW). Furthermore, the optimized device keeps the same spectral characteristics without introducing excessive voltage droop.

Document code: A **Article ID:** 1673-1905(2019)02-0113-4

DOI https://doi.org/10.1007/s11801-019-8113-6

Infrared light emitting diodes (LEDs) have important applications in vast fields, such as meteorology, security surveillance, infrared remote sensing, environmental monitoring, transducer/sensor and night lighting[1,2]. Especially, infrared LEDs at 940 nm have an advantage over others in the field of anti-interference, therefore they have been widely applied to remote sensing, inducing and intelligent systems[3]. At the same time, devices at 940 nm can partly replace those at 850 nm for security surveillance. The early infrared LEDs were mainly fabricated using GaAs homo PN junction to excite and emit infrared light by liquid phase evaporation (LPE) method. There are some shortcomings, such as thicker epitaxial layer, poor uniformity and repeatability, hence the cost is high and it is hard to mass production.

Because of the limitation of the packaging and circuit board, packaged infrared device with a single junction has much lower radiation power per unit area. People have made many efforts to improve radiation power under the fixed packaging body by using dual PN junctions design. Recently, dual-junction infrared chips with high efficiency have been applied to face recognition, iris recognition, smart driverless car system fields, as the dual-junction infrared device with high power can effectively reduce packaging size and cost[4,5].

As III-V group compound semiconductor, GaAs-based devices have been widely used, but pursuing high efficient performance on these device still attracts people's attention[6-10]. It is very necessary to optimize the epitaxy structure to improve optoelectric properties[11,12].

In this paper, epitaxial growth of GaAs/AlGaAs-based 940 nm infrared LEDs with dual junctions is carried out with varying doping concentration and constituents of $Al_xGa_{1-x}As$, and then the optoelectric properties of dual-junction infrared LEDs are studied. The favorable parameters are obtained, which are the hole concentration of P^{++} layer up to 1×10^{20} cm^{-3} and the electron concentration of N^{++} layer up to 5×10^{19} cm^{-3} in tunneling region, and the alloyed composition of the tunneling junction region of $Al_{0.2}Ga_{0.8}As$.

All the epitaxial growths in this paper were on 10.16 cm n-GaAs substrate with a horizontal reactor operating at a pressure of 5.6×10^3 Pa by using K475i MOCVD device in Veeco Ltd. Trimethylgallium [$(CH_3)_3Ga$, TMGa], trimethylindium [$(CH_3)_3In$, TMIn] and trimethylindium [$(CH_3)_3Al$, TMAl] were used for Ga, In and Al precursors, respectively. AsH_3 and PH_3 were used as group V sources, and SiH_4 was used for the n-type doping source. Traditional wafer structure of 940 nm LED is shown in Fig.1(a). After loading into the reactor, GaAs substrates were thermally cleaned in AsH_3 ambient for 10 min at 700 °C, a GaAs buffer layer was

* This work has been supported by the National Key Research and Development Program of China (No.2017YFB0403101), and the National Natural Science Foundation of China (No.61474096).

** E-mail: xhzeng@yzu.edu.cn

grown, and then the epilayer AlGaInP with thickness of 500 nm was grown on the buffer layer. Then N-GaAs contact layer, N-AlGaAs current extension layer, N-AlGaAs limit layer, active layer, P-AlGaAs limit layer, P-AlGaAs current extension layer, P-GaInP transition layer, P-GaP Ohm contact layer were grown in sequence[13]. Here, the active layer was composed of four pairs of alternating growth InGaAs and AlGaAsP layer, as shown in Fig.1(a).

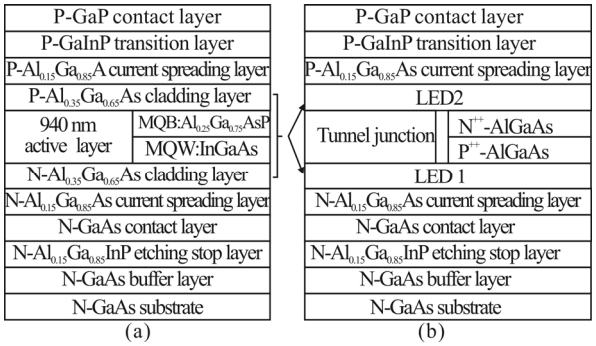

Fig.1 940 nm LED epitaxial structure with (a) a single junction and (b) double junctions

For the dual-junction 940 nm LED, the layout is displayed in Fig.1(b)**.** The wafer is grown in the sequence of GaAs substrate, GaAs buffer layer, AlGaInP layer, N-GaAs contact layer, N-AlGaAs current extension layer, LED1, tunnel junction, LED2, P-AlGaAs current extension layer, P-GaInP transition layer and P-GaP Ohm contact layer. Both LED1 and LED2 are composed of the N-AlGaAs limit layer, active layer and P-AlGaAs limit layer, and the tunneling junction is a heavy doped P^{++}-AlGaAs layer and an N^{++}-AlGaAs layer[14]. For the convenient comparison, except for the listed changes, the rest of them are the same as those in the single junction structure.

The effect of doping concentration and the constituents Al_xGaAs_{1-x} of LED tunneling junction with dual junctions on optoelectronic properties were studied, where the doping concentration of the tunneling junction was identified by growing single layer, and the Al constituent was controlled by the source flux. After growth of the wafers, chips with a size of 190.5 μm×190.5 μm can be obtained by chip processing. Finally, contrast results of the traditional and dual-junction LEDs on the device properties are carried out, and their current-voltage (*I-V*) characteristics and current-power (*I-P*) relations can be obtained.

Appropriate doping medium is crucial to obtain the expected tunneling junction. In the experiment, the p-type doping was obtained by using CBr_4 as doping sources, because C-doping has high activating rate, and has a wide range of concentration of 10^{17}—10^{21} cm^{-3}, which can be accurately controlled. Furthermore, carbon has a very low impurity diffusion coefficient and a good heat stability. Here, the n-type doping is an ordinal method, i.e., Si-doping. Optimizing doping concentration in tunneling junction is very necessary. Because only enough doping concentrations can guarantee small voltage rise under backward bias current, on the contrary, the higher doping concentration will influence the crystallinity of the source layer. Therefore, optimal doping concentration can ensure better performance of LED with dual junctions. Firstly, the wafer with dual junctions was grown with concentration of 2×10^{19} cm^{-3} for both P^{++} and N^{++}. The LED device reveals a voltage of 6.13 V at injection current of 50 mA, which is quite larger than that of the single junction LED (1.4 V). The main reason for the higher voltage is that the doping concentration of the tunneling junction is not high enough, leading to the Fermi energy locating in the forbidden band, and the carriers are hard to tunnel.

Then, wafers were grown with a fixed N^{++} doping concentration of 2×10^{19} cm^{-3} and different P^{++} concentrations of 2×10^{19} cm^{-3}, 6×10^{19} cm^{-3}, 1×10^{20} cm^{-3} and 5×10^{20} cm^{-3}. Their photoelectric parameters are shown in Fig.2. At injection current of 50 mA, the voltage drops from 6.13 V to 2.94 V and the output power increases from 21.5 mW to 24 mW with P^{++} concentrations increasing from 2×10^{19} cm^{-3} to 5×10^{20} cm^{-3}. From Fig.2, we find that both the voltage and output power saturate with P^{++} concentration over 1×10^{20} cm^{-3}.

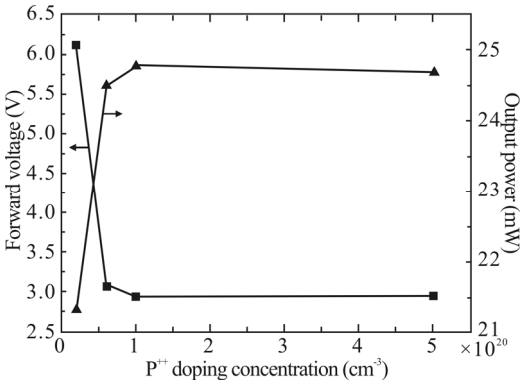

Fig.2 Photoelectric parameters of LEDs with different concentrations in P^{++} layer and fixed N^{++} doping concentration of 2×10^{19} cm^{-3}

Therefore, a fixed P^{++} doping concentration of 1×10^{20} cm^{-3} is used to further optimize N^{++} concentration. Two wafers with N^{++} concentrations of 5×10^{19} and 1×10^{20} cm^{-3} were grown, and the relations of the voltage and output power with N^{++} concentration at injection current of 50 mA are studied, which are shown in Fig.3. Both the voltage and the output power increase slightly with the increase of N^{++} concentrations. So, the doping concentrations are chosen as 5×10^{19} cm^{-3} for N^{++} and 1×10^{20} cm^{-3} for P^{++} in the following experiments.

In order to obtain higher optoelectric conversion efficiency, we make use of double-junction LEDs, which should satisfy both the lattice matching and reasonable band gap alignment. Furthermore, the tunneling junction connecting two LEDs should have excellent transparency and low impedance[15]. Here, we make use of $Al_xGa_{1-x}As$ as homo tunneling junction to connect two

LEDs. As the $Al_xGa_{1-x}As$ compounds with different contents Al have different band gaps, it is important to optimize the value of x[16].

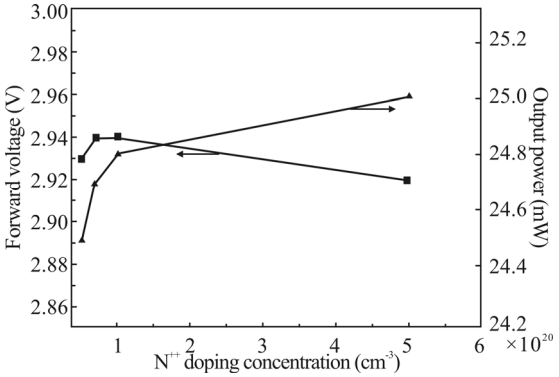

Fig.3 Photoelectric parameters of LEDs with different concentrations in N^{++} layer and fixed P^{++} concentration of 1×10^{20} cm^{-3}

Considering the above results, we grown three kinds of wafers at fixed doping concentrations of 5×10^{19} cm^{-3} for N^{++} and 1×10^{20} cm^{-3} for P^{++}, with the tunneling junction as $Al_{0.1}Ga_{0.9}As$, $Al_{0.2}Ga_{0.8}Al$ and $Al_{0.3}Ga_{0.7}As$. Their photoelectric properties are displayed in Fig.4. Fig.4 shows that both the output power and forward voltage of the device increases with x in $Al_xGa_{1-x}As$. To compensate the output power and forward voltage, we regard $Al_{0.2}Ga_{0.8}Al$ as a better choice.

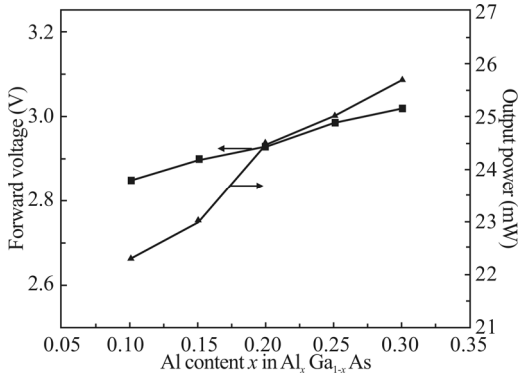

Fig.4 Photoelectric parameters of LEDs with different tunnel junction materials and the fixed doping concentrations of 5×10^{19} cm^{-3} for N^{++} and 1×10^{20} cm^{-3} for P^{++}

I-V characteristics of single and double tunneling junction LEDs at injection current of 50 mA are shown in Fig.5, where the parameters are used as obtained above. It shows that the forward voltage is 2.93 V for the double tunneling junction LED, which is 2.08 times larger than that of single junction device. As there are two source PN junctions in double tunneling junction LED, voltage droop induced from the series resistance and reverse tunneling junction is little in comparison with that of the traditional single junction device.

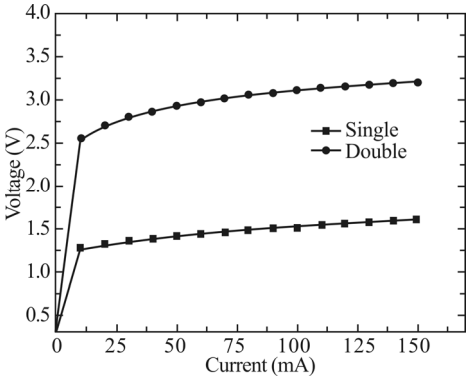

Fig.5 *I-V* characteristics of single and double tunneling junction LEDs

At the same time, the changes of output power with current were carried out. Fig.6 shows the relations of current and power for single and double tunneling junction LEDs. It shows that at injection current of 50 mA, the output power is 24.5 mW for double tunneling junction LED, it is 104% larger than that of the single junction (12 mW), and 118% larger than the reported result of 11.2 mW. At the same time, the emission wavelength at 940 nm for the double tunneling junctions is identical to the single one, meaning that the tunneling junction has no effect on the emission wavelength. The optoelectric performance indicates that it is an efficient way to improve the radiation power of LED by using double tunneling junctions.

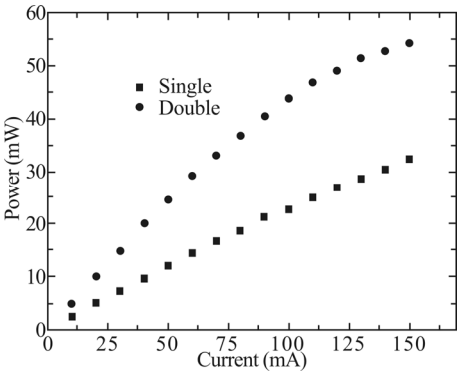

Fig.6 *I-P* characteristics of single and double tunneling junction LEDs

In summary, by using metalorganic chemical vapor deposition (MOCVD), 940 nm LEDs with double tunneling junctions are optimized by changing different tunneling doping concentrations and constituents. The optimal design for tunneling region is obtained, where the hole concentration in P^{++} layer is up to 1×10^{20} cm^{-3}, the electron concentration in N^{++} layer doping is up to 5×10^{19} cm^{-3}, and the constituents of the tunneling junction region is $Al_{0.2}Ga_{0.8}As$. In comparison with the traditional single junction LED, the radiation power of LED with double tunneling junctions is doubled, and the forward voltage 2.93 V of the double tunneling junction

LED is 2.08 times larger than that of single one. The double tunneling junctions don't induce an additional voltage droop, moreover the emission wavelength at 940 nm is identical to the single one. Therefore, it is an efficient way to improve the radiation power of LED by using double tunneling junctions.

References

[1] A. V. Zinovchuk, O. Yu. Malyutenko, V. K. Malyutenko, A. D. Podoltsev and A. A. Vilisov, J. Appl. Phys. **104**, 033115 (2008).

[2] D .P. Xu, M. D' Souza, J.C. Shin, L.J. Mawst and D. Botez, J. Crystal Growth **310**, 2370 (2008).

[3] D. K. Kim, H. J. Lee, Won-Chan An , H. G. Kim and L. K. Kwac, J. Korean Phys. Society **72**, 1020 (2018).

[4] H. D. Lu, B. Zhang and F. M. Guo, Opt Quant Electron **48**, 181 (2016).

[5] Z. Cevher, P. A. Folkes, H. S. Hier, B. L. VanMil, B. C. Connelly, W. A. Beck and Y. H. Ren, J. Appl. Phys. **123**, 161512 (2018).

[6] D. Ban, H. Luo, H. C. Liu, Zbigniew R. Wasilewski and Margaret Buchanan, IEEE Photonics Technol. Lett. **17**, 1477 (2005).

[7] D. Das, H. Ghadi, B. Tongbram, S.M. Singh and S. Chakrabarti, J. Lumin. **192**, 277 (2017).

[8] I. E. Cortes-Mestizo, E. Briones, C.M. Yee-Rendón, L. Zamora Peredo, L.I. Espinosa-Vega, R. Droopad and Victor H. Méndez-García, J. Crystal Growth **477**, 59 (2017).

[9] R. A. Herrera and C. A. Alvarez Ocampo, J. Nonlin. Optical Phys. & Mate., **26**, 1750031 (2017).

[10] T. Walther and A.B. Krysa, J. Microscopy **268**, 298 (2005).

[11] D. K. Kim and H. J. Lee, J. Nanoscien. and Nanotechn. **18**, 2014 (2018).

[12] T. Kawazu, T. Noda and Y. Sakuma, Appl. Phys. Lett. **112**, 072101 (2018).

[13] J. Souto, J. L. Pura, A. Torres, J. Jiménez, M. Bettiati and F. J. Laruelle, Microelectron. Reliability **64**, 627 (2016).

[14] Z. Z. Zhang, Z. L. Fu, X. G. Guo and J. C. Cao, Chin. Phys. B **27**, 030701 (2018).

[15] Cheng-Han Wu and Chao-Hsin Wu, Appl. Phys. Lett. **105**, 171104 (2014).

[16] J. Thoma, B. L. Liang, L. Lewis, S. P. Hegarty, G. Huyet and D. L. Huffaker, Appl. Phys. Lett. **102**, 113101 (2013).